Eleventh International Conference on CFD in the Minerals and Process Industries
CSIRO, Melbourne, Australia
7-9 December 2015

INCORPORATION OF FINITE BUBBLE SIZE EFFECTS IN A CFD MODEL OF AN ALUMINIUM REDUCTION CELL

M. Philip SCHWARZ[1*], Yuqing FENG[1], Peter J. WITT[1] and Mark A. COOKSEY[1]

[1] CSIRO Minerals Resources, Clayton, Victoria 3169, AUSTRALIA
*Corresponding author, E-mail address: Phil.Schwarz@csiro.au

ABSTRACT

Two-fluid (Eulerian–Eulerian) simulation of bubbly flow normally assumes that bubble size is smaller than the computational cell size, although the formulation should continue to be valid as mesh is refined below bubble size. In some situations, one may need to use a mesh that is finer than the bubble size, but it is argued that the standard two-fluid equations fail in such situations. Averaging of the Navier–Stokes equations is analysed to understand this effect, and equations that account for the finite size effect are derived. As an example, finite bubble size effects are shown to be important in a simulation of a water model of an aluminium reduction cell. In this case, bubbles are generated on the lower face of submerged anodes, slide to the edge of the anodes and rise to the liquid surface. The bubble plumes at the side of the anodes are predicted to be too narrow unless finite size effects are taken into account. An approximate method for correcting the usual two-fluid equations is trialled and is shown to predict void distribution in qualitative agreement with observations from the water model.

NOMENCLATURE

C_{FS} finite size effect coefficient, used in eqn. (10)
d particle diameter
$\mathbf{F}_i$ momentum source on phase i due to body forces
M_i momentum source due to interfacial transfer
n number density of particles
n_k number density of k-th size fraction of particles
N_p number of particles
p pressure
p_c pdf of particle centres
$\mathbf{r}$ position vector (x,y,z)
R radius of particle
t time
$\mathbf{u}_k$ averaged velocity of phase k
$\mathbf{v}_k$ instantaneous velocity of phase k
V volume
V_p volume of particle

α average void fraction
ρ_k density of phase k
μ_{eff} effective eddy viscosity
ϕ_k characteristic phase function

INTRODUCTION

The two-fluid (commonly called the "Eulerian–Eulerian") method for simulating two-phase flows such as bubbly flow is based on solving sets of continuity, momentum and energy equations for each phase, with the equations for each phase defined over the entire domain. The method should be distinguished from other multi-material Eulerian–Eulerian methods which solve for instantaneous equations defined only over the part of the domain occupied by the particular phase.

The equations of the two-fluid model are derived by averaging (usually ensemble-averaging) of the local instantaneous equations for single-phase flow (Drew and Passman, 1999; Kataoka and Serizawa, 1989). Two sets of balance equations for mass and momentum are obtained. While the assumption is usually made that the dispersed phase (particle, bubble or drop) size is much smaller than the control volume used in the averaging, the partial differential equations so derived should be generally valid, so that, in particular, as the mesh size in a simulation is reduced below the bubble size, the solution should be independent of mesh size.

Feng et al. (2015) have pointed out a situation in which this is not true: when relatively large bubbles released at the bottom edge of an anode, the width of the computed voidage distribution representing the bubble plume reflects the (narrow) initial width of the bubble at the anode corner, rather than the (much wider) diameter of the bubbles when they equilibrate to their rising shape.

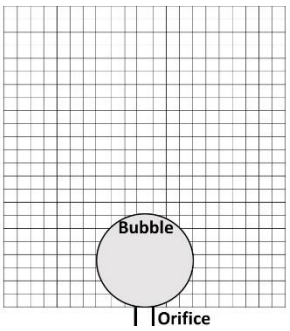

Figure 1: Schematic diagram of bubble formation at an orifice illustrating the issue that arises when bubble size is larger than mesh size..

This issue was encountered several years ago by researchers simulating gas injection into liquids: the initial bubble size formed at nozzles was often much larger than the nozzle diameter, and indeed larger than the desired mesh size. This is illustrated schematically in Figure 1. In these cases, if the gas inlet boundary condition is set on the orifice only, the initial voidage distribution just above the orifice does not correctly reproduce the voidage distribution of bubbles generated at the orifice. To overcome this issue, the

boundary condition for the voidage distribution was taken to have the width of bubbles formed at the nozzle (Schwarz and Turner, 1988; Davidson, 1990; Schwarz, 1996). That is, it was assumed that the gas enters the bath with the bubble velocity through an *apparent* orifice having a diameter equal to the bubble diameter, which can be estimated by empirical and theoretical correlations.

At the time, researchers treated the bubble injection issue as an exceptional case to be solved by special treatment. Indeed one may think that the cause of the problem is the neglect of surface tension forces. In fact, as we will see, the issue is more general, and arises from the neglect of critical information about phase structure (and surface tension is just one of the factors influencing phase structure).

In principle, ensemble averaging should be capable of taking into account such issues. However, up until now, this has not been done, probably because the phase structure has been assumed to be on a scale smaller than the computational mesh. Drew (1983) admits that there has been no general treatment of interfacial geometry in the two-fluid model formulation, with the best attempts being the derivation of equations for conservation of interfacial surface area (e.g., Ishii, 1975; Kocamustafaogullari and Ishii, 1995; Delhaye, 2001).

It may be argued that when phase structure is larger than mesh size, simulation can be carried out more accurately using a Volume of Fluid (VOF) approach. However, simulation of large-scale complex multi-phase industrial applications is still very challenging task for a VOF method, particularly as many simulations may be required for optimisation purposes in an industrial context. Until such simulations are possible in a reasonable time-frame, a more pragmatic approach needs to be taken: Schwarz and Feng (2015) describe a multi-scale approach where information from detailed VOF models of the sort described by Zhang et al. (2013) and Zhao et al. (2014) are used to improve closures required by two-fluid simulations of the sort described by Feng et al. (2015).

In this paper we analyse the cause of the problem outlined above, derive equations which should overcome the issue and give an example of the problem in an industrial case of importance, namely bubbles rising beside an anode in an aluminium reduction cell.

TWO-FLUID MODEL AVERAGING

Volume Fraction Averaging

In order to explain the essence of the issue without confusing the matter with surface tension effects, we consider the case of non-deformable particles. Whether these are solid, liquid or gaseous is not relevant, though solid particles are most easily comprehended. The discussion can be extended to deformable particles, though the physical issue of surface tension must be accounted for.

First consider averaging of the continuity equations. The local instantaneous equations of the conservation of mass are:

$$\frac{\partial(\phi_k \rho_k)}{\partial t} + \nabla \cdot (\phi_k \rho_k \mathbf{v}_k) = 0 \qquad (1)$$

(Kataoka, 1986; Kataoka and Serizawa, 1989), where they define a characteristic function, ϕ_k, of phase k as unity if that phase is present at the point, and zero otherwise. The space or time-averaged value of ϕ_1 corresponds to the "void fraction" if phase 1 is the bubble phase.

Kataoka and Serizawa (1987) carry out averaging of eqn. (1) as statistical averaging, though the averaging could equally well be spatial or temporal. In this averaging process, there are no assumptions made about the phase structure, so the averaging at each point is independent of that at other points.

Consider two points A and C separated by a distance greater than the particle diameter. Then the average volume fractions at these two points will be statistically independent (apart from physical interaction effects between particles, such as clustering, which are explicitly accounted for by hydrodynamics, inter-particle forces, etc.).

Now consider the averaging procedure for volume fraction at two points, A and B, which are closer together than the particle diameter, *d*. Then the values of the statistical average volume fraction at points A and B are not statistically independent. For example, if the separation is d/4, then it is quite likely that if there is particle phase at point A, there will also be particle phase at point B at the same realisation (or time instant in the case of temporal averaging). Indeed, as the separation becomes very much smaller than the diameter, the volume fractions at A and B become more correlated.

Now the essence of the concept being proposed in this section is that the averaging process, as conventionally performed, is based on the assumption that the volume fraction at each point is *a priori* statistically independent of that at all other points, even at points located very close. Of course, the hydrodynamics will usually result in the solved values of average volume fractions at neighbouring points being correlated: for example, advection and turbulent diffusion mean that it is likely that neighbouring points will have similar volume fraction. But this is as a result of the solution of the hydrodynamic equations; the raw two-fluid equations involve an assumption that the volume fractions at neighbouring points are uncorrelated.

Another way of expressing this concept is that, when the dispersed phase is composed of finite size entities (particle, bubbles, droplets), there are additional constraints that are not accounted for in the standard multi-fluid equations. Furthermore, these constraints have so far not been accounted for within the physical forces or terms involved in the solution of the two-fluid equations. As a result, the constraints are usually not accounted for at all in the two fluid simulation.

To underline this last point, it is useful to point out that the effect being considered has no relationship with physical forces such as lift force, collisional dispersion of particles, turbulent diffusion, or any of the other forces that are included from time to time. The effect being considered simply arises from the fact that the dispersed phase is comprised of finite sized entities. In the case of non-deformable particles, the size of the entities (and perhaps their shape, if non-spherical) is known *a priori*. But even in cases where the entities can be subject to break-up and coalescence (in which case the size is not known *a priori*) the effect is still present.

Distribution of particle centres

With regard to the discussion in the previous sub-section, it is important to draw a distinction between the (average) volume fraction at a point, $\alpha(x,y,z)$ and the number density of particles, which can be characterised by a probability density function of particle centres, $p(x,y,z)$.

The number of particle centres in a volume dV at a point (x,y,z) is $p_c(x,y,z)\,dV$.

On the other hand, the volume of dispersed phase in the volume dV is $\alpha(x,y,z)\,dV$

At a point $\mathbf{r} = (x,y,z)$, the volume fraction can be found by summing the contributions from all particles with centres closer than R, the particle radius. So

$$\alpha = \int_{\substack{\text{all } \mathbf{s} \text{ within} \\ \text{sphere} \\ \text{radius } R}} pc(\mathbf{r}+\mathbf{s})dV(\mathbf{r}+\mathbf{s}) \qquad (2)$$

It is worth noting that in the calculation of forces and other quantities within CFD simulations, it is common to calculate the number of particles in a volume ΔV as

$$N_p \approx \alpha(x,y,z)\Delta V / V_p \qquad (3)$$

where V_p is the volume of a particle. This is equivalent to assuming that p_c is constant over a sphere of radius R, so that eqn. (2) becomes

$$\alpha \approx \tfrac{4}{3}\pi R^3 p_c \qquad (4)$$

It must be emphasised that eqn. (3) is not in general a valid expression for the number of particle centres in the volume ΔV, though the number of particles will tend to this quantity as the particle volume becomes small compared with ΔV. In CFD implementations, the volume ΔV is generally associated with the cell volume, so eqn. (3) for the number of particle centres is valid when the particle size is much smaller than the grid dimensions.

On the other hand, if the particle size is of order of or larger than the grid dimensions, then eqn. (3) is only approximate. The reason for this is that the average volume fraction is defined in terms of the statistical probability of the presence of dispersed phase at a point, not in terms of particle centres. When particle size is larger than the grid dimension, the spatial extent of dispersed phase will be wider than the spatial extent of particle centres.

Indeed it is possible (though usually unlikely) that, in a particular volume dV, the volume of dispersed phase, $\alpha(x,y,z)\,dV$, could be significant, while the number of particle centres, $p_c(x,y,z)\,dV$, is zero.

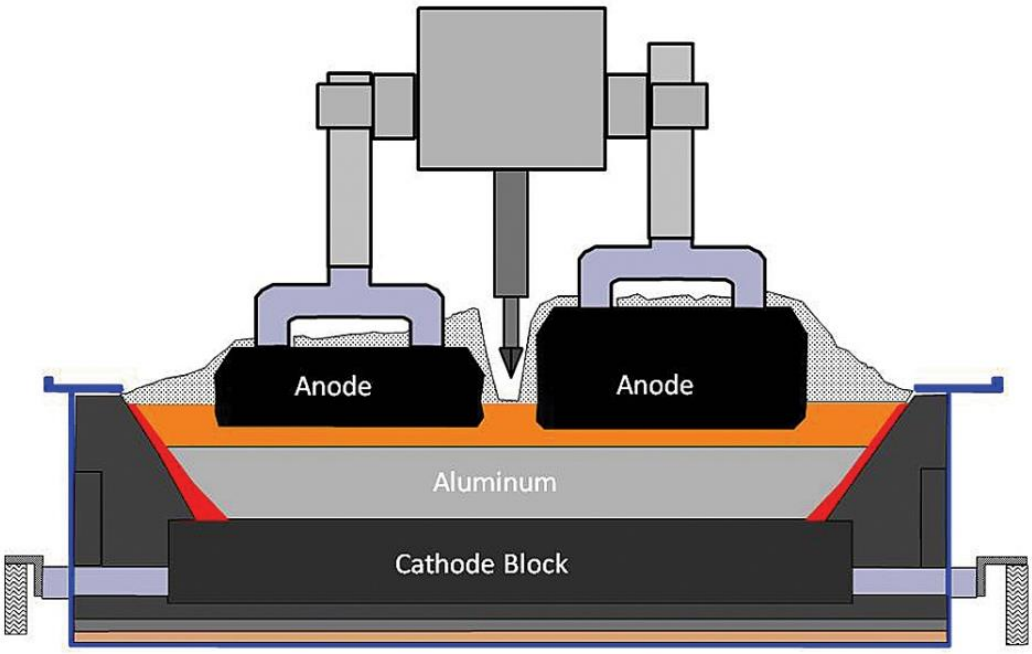

Figure 2: Schematic diagram of Hall-Héroult cell

Eqn. (3) for the number of particles in a volume ΔV is routinely used in determining forces and other quantities within two-fluid CFD simulations. For example, drag terms are based on this assumption (at least when based on generalisations of drag of individual bubbles or particles (Smith, 1998)), as are interfacial reaction rates, and so on. Furthermore, break-up and coalescence rates for population balance models are all based on this equation (see, for example, eqn. (75) of Wang et al. (2008)).

The question arises as to whether this effect is actually significant. Fortunately it appears that the effect is usually negligible, but there are situations, such as that presented here, where the effect is very important.

Model modification for finite sized bubbles

To better appreciate the effect, we examine the mass conservation equations in the two fluid model formulation. Kataoka and Serizawa (1989) give the average mass conservation equation for phase k, in the incompressible situation with no phase change, as

$$\frac{\partial \alpha_k}{\partial t} + \nabla \cdot \left(\alpha_k \mathbf{u}_k \right) = 0 \qquad (5)$$

where $\mathbf{u}_k$ must be read as the average phase velocity, in their case phase weighted average. As mentioned previously, the volume fraction variables are determined by statistically averaging at a point, the instantaneous phase variable, ϕ_k, defined by Kataoka and Serizawa (1989) as unity if the phase is present at that point, and zero otherwise.

On the other hand, the equation for the number density of particles, *n*, is

$$\frac{\partial n}{\partial t} + \nabla \cdot \left(n \mathbf{u}_p \right) = 0 \qquad (6)$$

Here, $\mathbf{u}_p$ must be read as the average velocity of particle centres, which in population balance models is always taken to be the same as the average phase velocity. In this case, for the number density of particles, *n*, is equal to the probability density distribution of particle centres, p_c.

One possible procedure for obtaining the void fraction with account taken for finite particle size effects, would be to solve for number density of particle centres, eqn. (6), instead of solving for the usual mass conservation equation for the dispersed phase, eqn. (5). Then the corrected void fraction can be determined by convolving the number density with the mass distribution for an individual particle, which for a uniform density spherical particle, amounts to performing the calculation given in eqn. (2).

The approach described above has the advantage that it can be easily extended to the case of multiple size fractions:

$$\frac{\partial n_k}{\partial t} + \nabla \cdot \left(n_k \mathbf{u}_k \right) = 0 \qquad (7)$$

where n_k is the number density of the k-th size fraction.

Coalescence and breakup could be accounted for by source terms in the same way as in population balance modelling. Note however that this approach is different from the way a population balance is normally applied, namely as equations additional to the phase conservation equations.

In order to complete the set of equations used in this approach, it is also necessary to apply the phase constraint in the derivation of the momentum conservation equations. Just as the phase at nearby points is correlated when particles are relatively large, so too will be the velocity. These equations will be derived in a future paper. To apply this approach, it would be necessary to revisit and modify the usual solution methods for the two-fluid equations.

An alternative approach would be to propose additional semi-theoretical terms for the standard two-fluid equations, in much the same way as terms have been presented to account for complex effects such as lift force, turbulent dispersion, bubble-induced turbulence, the so-called "lubrication force", and so on. These terms have not been determined on the basis of rigourous averaging, but rather in a semi-theoretical, even heuristic fashion (see, for example, the discussion by Sokolichin et al., 2004). There are often various different expressions available in the literature, and they generally involve empirical parameters that must be determined from experiment.

In the case of the finite size effect described above, it is likely that a suitable term would be of a diffusion or dispersion type, given that the effect involves a convolution with the mass distribution of a particle (eqn. (2)).

In this work, we take an approximate approach of adding a dispersion force to ensure that the width of the distribution of dispersed phase volume fraction is consistent with bubble size.

MODEL DESCRIPTION

The effect described in the previous section will be illustrated using a model of the high temperature electrolytic cell (the Hall–Héroult cell) used for reducing alumina to produce aluminium (Grjotheim and Welch, 1988). A schematic diagram of such a cell is given in Figure 2. Alumina is dissolved in a molten mixture of cryolite and aluminium fluoride, and current is passed through it from submerged anodes to a cathode which forms the base of the cell. The electrolysis causes liquid aluminium metal to be deposited on the cathode, while carbon dioxide is produced at the anode. It is believed that the gas coalesces to form large bubbles flattened against the lower anode surface. The bubbles slide to edges of each anode, where they subsequently rise rapidly through the electrolyte to the surface.

There are many complex modelling issues involved in comprehensive simulation of aluminium reduction cells, and these have been described by Eick et al. (2015). The circulation of the electrolyte caused by bubble drag is the main subject of the modelling described here. This aspect of cell dynamics has been investigated numerically by Feng et al. (2010, 2015): the electrolyte flow is important for several reasons related to the operation and energy requirements of the cell, as described by Feng et al. (2015).

The two–phase (gas–liquid) model of the cell that is the subject of this work has been described in detail by Feng et al. (2015). The model is of an air–water model of an aluminium cell, with three anodes. The physical model, illustrated in Figure 3, consists of three anodes of a scale typical of a modern prebake cell, though the dimensions and conditions do not correspond to any actual operation. The physical model was constructed in Perspex to facilitate PIV (Particle Image Velocimeter) measurements of velocity, as described in detail by Cooksey and Yang (2008). Each anode is 1300 mm × 650 mm × 600 mm in size, with 160 mm of the anode submerged. The height of electrolyte beneath the anodes is 40 mm. Centre and side channel widths are 120 mm and 240 mm respectively, and tap-end and duct-end channel widths are 160 mm and 40 mm respectively.

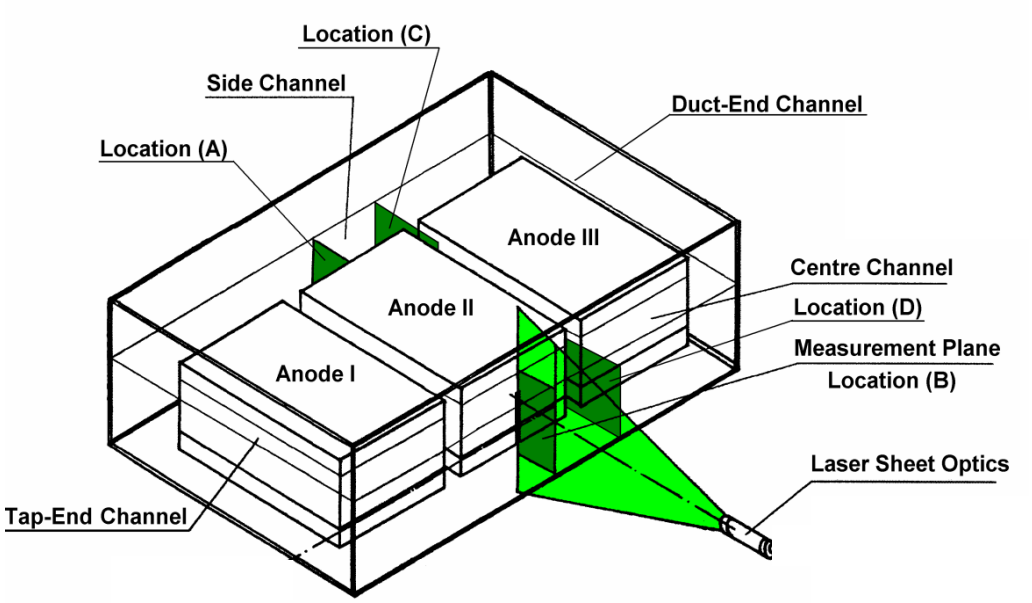

Figure 3: Schematic diagram of three-anode water model of an aluminium reduction cell, simulated by Feng et al. (2015).

The CFD model uses the two-fluid approach, with a set of continuity and momentum equations for each phase, *i*:

$$\nabla \cdot \left(\alpha_i \rho_i \mathbf{u}_i\right) = 0 \tag{8}$$

$$\nabla \cdot \left(\alpha_i \rho_i \mathbf{u}_i \mathbf{u}_i\right) = -\alpha_i \nabla p + \nabla.\left(\alpha_i \mu_{\text{eff}} \nabla \mathbf{u}_i\right) + \mathbf{F}_i + \mathbf{M}_i \tag{9}$$

where α_i is the volume fraction of phase *i* (either gas or water), ρ_i and $\mathbf{u}_i$ are the density and vector velocity for phase *i*, and *p* and μ_{eff} are the pressure and effective turbulent viscosity. The term $\mathbf{F}_i$ describes momentum sources due to external body forces, in this case buoyancy. The term $\mathbf{M}_i$ describes the interfacial momentum transfer between phases including the drag force and inter-phase turbulent dispersion force. Turbulence is modelled using the *k-ε* equations, with source terms for bubble-induced turbulence.

As gas releases from the bottom of the anodes, buoyancy causes it to rise very rapidly from the bottom corners of the anodes upwards into the channels surrounding the anodes. The rapid rise results in gas remaining in a narrow layer close to the anode side walls in the simulations – narrower than the size of bubbles. In order to account for the finite size of bubbles, i.e., to ensure that the plume width is consistent with bubble diameter, the voidage distribution at the anode corner is artificially widened by an additional diffusion term so that the voidage width there is approximately equal to the bubble size, as determined from Weber number considerations. Feng et al. (2015) use such a Weber number criterion to show that the expected bubble size in the side and centre channels of the water model is approximately 40 mm, and this is in accord with visual observations of the air-water model during operation. On the other hand, it should be noted that the horizontal width of the (hexahedral) cells in the side channel is only 24 mm.

The force term is taken to be of a form analogous to that of the turbulent dispersion force (Burns et al., 2004):

$$\mathbf{M}_l^{\text{FS}} = -\mathbf{M}_g^{\text{FS}} = -C_{\text{FS}}\left(\frac{\nabla \alpha_g}{\alpha_g} - \frac{\nabla \alpha_l}{\alpha_l}\right) \tag{10}$$

where the finite size effect coefficient, C_{FS}, must be determined empirically to ensure that the void fraction width is consistent with bubble size.

As mentioned in the introduction, simulation of such a system can undoubtedly be more accurately simulated using a Volume of Fluid (VOF) approach. Indeed this approach has also been pursued by the authors (Zhang et al., 2013, Zhao et al., 2014), albeit only for a thin slice through a channel, because of the major computational requirements. Industrial simulation of an entire aluminium cell, which comprises of order 20 anodes, is still a very challenging task for a VOF method, particularly as many simulations may be required for optimisation purposes in an industrial context. Until such simulations are possible in a reasonable time-frame, a more pragmatic approach, such as the multi-scale method described by Schwarz and Feng (2015) needs to be taken.

RESULTS

Figure 4 shows computed void fraction contours on a plane through the centre channel, halfway along the middle anode (Location B in Fig. 3). The top plot shows the results without account for finite bubble size effects and the bottom plot shows results when finite bubble size effects are taken in account.

In the top plot, the gas hugs the side of the anode in an unrealistically narrow "plume", only broadening slightly as the gas rises as a result of turbulent dispersion. The width of the plume is narrower than the bubble size, which is clearly unphysical. As described in the section on Two Fluid Model Averaging, the reason for this behaviour is that the known bubble size is not taken into account as a constraint in the standard two-fluid equations. Of course bubble size enters into the expressions for various forces such as drag, but these do not provide the required constraint.

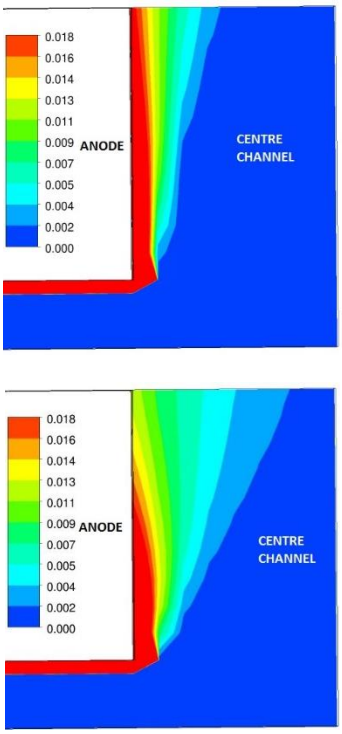

Figure 4: Comparison between simulation result without (top) and with (bottom) finite bubble size effects. Colour contours show void fraction for the bubble plume in the centre channel halfway along the middle anode (Location B in Fig. 3).

In the bottom plot of Figure 4, the bubble plume is much wider, and is qualitatively similar to the plume observed in the actual water model. It should be noted that the resultant plume widening does not directly result from the wider gas distribution imposed at the anode corner. In addition to this direct effect, the turbulence kinetic energy and velocity fields are also altered. For example, because of the wider gas distribution, the bubble induced turbulence source term is more widespread, leading to more turbulence, and consequently an even wider plume. Multiple coupled hydrodynamic interactions are responsible for generating the final bubble plume distribution.

Figure 5 shows a similar plot as Figure 4 but for the computed void fraction contours on a plane through the side channel, halfway along the middle anode (Location A in Fig. 3). The bottom plot shows the result of including the finite bubble size effect: the plume is substantially widened, as in the centre channel.

The same widening occurs in the tap-end and duct-end channels as a result of including the finite bubble size effect.

CONCLUSION

By analysing the two-fluid equations of mass conservation, it has been shown that the known bubble/particle size has an effect which has not hitherto been accounted for. This effect is usually small, but when bubble/particle size is larger than the computational mesh size, it is possible in some special situations for the effect to be important.

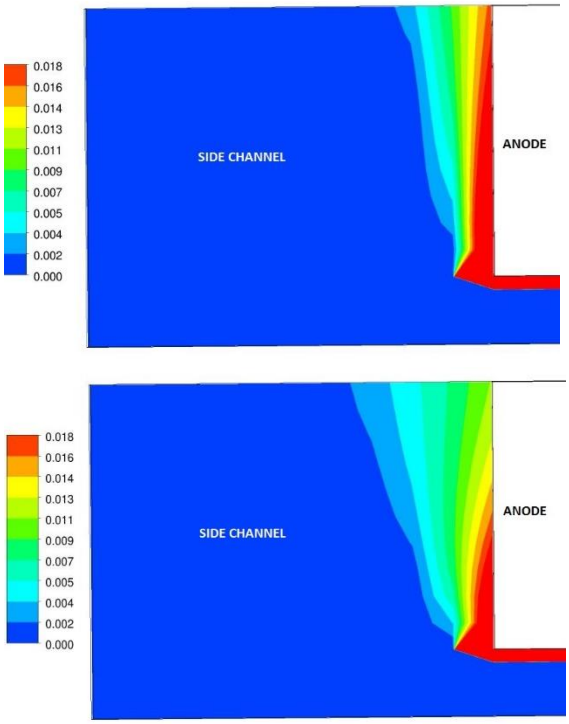

Figure 5: Comparison between simulation result without (top) and with (bottom) finite bubble size effects. Colour contours show void fraction for the bubble plume in the side channel halfway along the middle anode (Location A in Fig. 3).

An alternative approach to the standard two-fluid equations has been suggested to account for the finite particle size effect.

Furthermore, the effect has been illustrated in a two-fluid model of bubble flow in an aluminium reduction cell. An approximate technique for accounting for the effect, namely an additional dispersion force, has been shown to generate plume width in agreement with observations of an air-water model, whereas the standard two-fluid model equations generate unrealistically narrow plume width.

REFERENCES

BURNS, A.D., FRANK, T., HAMILL, I., and SHI, J.-M., (2004), "The Favre averaged drag model for turbulent dispersion in Eulerian multi-phase flows", *5th Inter. Conf. on Multiphase Flow, ICMF'04*, Yokohama, Japan, May 30–June 4, 2004, Paper No. 392.

COOKSEY, M.A. and YANG, W., (2006), "PIV measurements on physical models of aluminium reduction cells", *Light Metals 2006*, TMS, pp. 359–365.

DAVIDSON, M.R., (1990), "Numerical calculations of two-phase flow in a liquid bath with bottom gas injection: The central plume", *Appl. Math. Modelling*, **14**, 67–76.

DELHAYE, J.-M., (2001), "Some issues related to the modeling of interfacial areas in gas–liquid flows I. The conceptual issues", *C. R. Acad. Sci. Paris*, t. 329, Série II b, p. 397–410,

DREW, D.A., (1983), "Mathematical modelling of two-phase flow", *Ann. Rev. Fluid Mech*., **15**, 261–291.

DREW, D.A. and PASSMAN, S.L., (1999), "Theory of multicomponent fluids", *Applied Mathematical Sciences* 135. Springer.

EICK, I., BAI, W., EINARSRUD, K.E., FENG, Y., HUA, J., WITT, P.J., (2015), "Coupled multi-scale, multi-physics simulation framework for aluminium electrolysis", *Eleventh International Conference on Computational Fluid Dynamics in the Minerals and Process Industries*, CSIRO.

FENG, Y.Q., YANG, W., COOKSEY, M.A. and SCHWARZ, M.P., (2010), "Development of whole cell CFD model of bath flow and alumina mixing", *J. of Comput. Multiphase Flows*, **2**, 179–188.

FENG, Y.Q., SCHWARZ, M.P., YANG, W. and COOKSEY, M.A., (2015), "Two-phase CFD model of the bubble-driven flow in the molten electrolyte layer of a Hall-Héroult aluminum cell", *Metall. Mat. Trans. B*, **46**, 1959–1981.

GRJOTHEIM, K. and WELCH, B.J., (1988), Aluminium Smelter Technology, 2nd Edn., Aluminium-Verlag, Dusseldorf.

ISHII, M., (1975), Thermo-fluid dynamic theory of two-phase flow, Eyrolles, 1975.

KATAOKA, I., (1986), "Local instant formulation of two-phase flow*", Int. J. Multiphase Flow*, **12**, 745-758.

KATAOKA, I. and SERIZAWA, A., (1989), "Basic equations of turbulence in gas-liquid two-phase flow", *Int. J. Multiphase Flow*, **15**, 843-855.

KOCAMUSTAFAOGULLARI, G. and ISHII, M., (1995), "Foundation of the interfacial area transport equation and its closure relations", *Inter. J. of Heat and Mass Transfer*, **38**, 481–493.

SCHWARZ, M.P. and TURNER, W.J., (1988), "Applicability of the standard k-ε turbulence model to gas-stirred baths", *Appl. Math. Modelling*, **12**, 273–279.

SCHWARZ, M.P., (1996), "Simulation of gas injection into liquid melts", *Appl. Math. Modelling*, **20**, 41–51.

SCHWARZ, M.P. and FENG, Y.Q. (2015), "Pragmatic CFD modelling approaches to complex multiphase processes". *Progress in Applied CFD.* J.E. Olsen and S.T. Johansen (Eds.) SINTEF, pp. 25–38.

SMITH, B.L. (1998), "On the modelling of bubble plumes in a liquid pool", *Appl. Math. Modelling*, **22**, 773–797.

SOKOLICHIN, A., EIGENBERGER, G. and LAPIN, A., (2004), "Simulation of buoyancy driven bubbly flow: established simplifications and open questions", *A.I.Ch.E. J.*, 50, 24-44.

WANG, T., WANG, J.F. and JIN, Y. (2008), "A CFD–PBM Coupled Model for Gas–Liquid Flows", *AIChE Journal*, **52**, 126–140.

ZHANG, K., FENG, Y.Q., SCHWARZ, M.P., WANG, Z., COOKSEY, M., (2013), "Computational fluid dynamics (CFD) modeling of bubble dynamics in the aluminum smelting process", *Ind. Eng. Chem. Res*., 52, pp 11378–11390.

ZHAO, Z., ZHANG, K., FENG, Y., WITT, P., SCHWARZ, M.P., WANG, Z. and COOKSEY, M., (2014), "A numerical investigation of dominant factors affecting the bubble dynamics between air-water and CO2-cryolite systems", *19th Austral. Fluid Mech. Conf.*, Melbourne, 8-11 Dec. 2014.

